Off-Design Performance of Hypersonic Waveriders

Lyle N. Long*
The Pennsylvania State University, University Park, Pennsylvania 16802

Waveriders are being considered more and more as potential aerospace vehicles. There are several questions, however, regarding these configurations that must be answered before they can be considered viable designs. The most significant problems are related to aerothermal heating, propulsion integration, and off-design performance. This paper presents off-design performance predictions for two generic waveriders. The results are from a numerical method based on the nonlinear, inviscid Euler equations. Comparisons to experimental data are also shown.

Introduction

THE subject of this paper is the off-design performance of hypersonic waveriders. These vehicles are fairly well understood at their design Mach number and angle of attack, but their behavior at other conditions is not well documented. In addition, waveriders that have nonplanar or nonconical bow shocks[1] are also not well understood. After a brief discussion of some of the off-design problems encountered on waveriders, some numerical results will be presented. The results will be for two different waveriders and will be limited to inviscid flows.

With the recent resurgence of interest in hypersonic vehicles, waverider configurations are being proposed as effective hypersonic designs. Waveriders are vehicles that capture a bow shock along their leading edges; this eliminates flow around the leading edges[2] and captures the high-pressure air. In effect, the shock wave generated by thickness or volume is also used for lift. The result is a significantly higher lift coefficient for a given lift/drag (L/D) ratio than more conventional designs, or a higher L/D for a given lift coefficient. An increase in L/D can usually be equated with an increase in aircraft range or cross range.[3]

Kuchemann[2] describes how aircraft fall into one of three categories: wing body (or swept), slender, or waverider. An understanding of one class does not necessarily allow one to design an effective vehicle in another. Just as one could not have anticipated the design of the Concorde or the SR-71 in the 1930s, no one today can anticipate the ultimate hypersonic cruiser of the next century.

Wing-body aircraft are very effective at low speeds but are not well suited to supersonic flight. Slender configurations have subsonic leading edges at supersonic freestream conditions. As the Mach number is increased, this requirement produces vehicles that are too slender to be practical. If one must use supersonic leading edges, waveriders appear to be very effective, especially if one is interested in global flights in reasonable times (under 2 h).

Several excellent surveys of waveriders have been published[2,4-7]; therefore, few historical remarks on waveriders will be made. Although these vehicles have been thoroughly studied at their design conditions, off design they produce very complex flowfields and have not been analyzed in detail. Two exceptions are Squire's presentation[8] of a set of charts for the off-design characteristics of diamond and caret configurations and Jones' full-potential analyses.[9] Off-design behavior is typically determined from wind-tunnel tests, many of which are described in Refs. 2 and 4-7. Off-design performance is critical since many hypersonic configurations will not be point-design vehicles. With the recent advances in computational fluid dynamics (CFD), these flows can be analyzed in detail, including real gas and viscous effects. Until realistic waverider configurations are thoroughly studied at off-design conditions, they cannot be seriously considered as practical designs.

Some of the major phenomena that must be addressed before waveriders can be considered viable are the following: aeropropulsion integration, aerothermal heating, stability and control, nonconical or nonplanar bow shocks, shock-wave impingement, leading-edge vortices, degradation of theoretical performance due to viscous effects, effect of leading-edge radii, upper surfaces not aligned with freestream, and shock thickening due to Knudsen number effects. Most of these effects will only be described briefly here, and then some results for generic waverider configurations at off-design conditions will be shown.

Viscous effects will be critical to assess accurately aeropropulsion integration, aerothermal heating, shock/boundary-layer interactions, and separated flows. Townend[6] suggests that the heating problems (both the rate and the peak) may be less severe on waveriders than on flat delta wings with the same lower surface deflection angle.

For air-breathing vehicles, the inlets and nozzles may be essentially the entire fore and aft lower sections of the vehicle, respectively. Therefore, the aeropropulsion integration problem cannot be separated from the exterior aerodynamics of the vehicle. The hot reacting flows in the base region will be especially difficult to calculate or simulate experimentally due to the interaction of complex chemical kinetic effects and turbulent shear layers. Some of the problems associated with inlets for hypersonic vehicles are discussed by Molder,[7] Hunt et al.,[10] and more recently by Hemdan and Jischke.[11] Aerodynamic and inlet performance improvements due to fuselage cambering are discussed in Ref. 10.

The off-design location of shock waves can seriously impact performance, heat transfer, and propulsion integration. Conventional slender aircraft have leading edges swept inside the bow shock. Waveriders have a bow shock captured on their leading edges. On conventional vehicles, at Mach numbers greater than their designed values, the forebody bow shock can impinge upon the wing leading edges. This results in significant

Received July 28, 1987; revision received Nov. 30, 1989.

*Assistant Professor, Dept. of Aerospace Engineering. Member AIAA.

increases in local aerothermal heating unless the leading edges are highly swept.[12] One may not be able to sweep inlet-cowl leading edges, however, which means they must be actively cooled or incorporate high-temperature thermal protection systems. An excellent review of aerothermal heating is given in Ref. 13. Shock-wave systems on waveriders are described in Ref. 14.

Waveriders at Mach numbers above their design values will encounter a completely different type of shock impingement. Instead of impinging on the leading edges, the shocks may sweep across the upper and lower surfaces. This will cause very complicated shock/boundary-layer interactions and possibly high heating rates. Reference 15 presents a very comprehensive review of shock/boundary-layer interactions.

Stability and control of waveriders is a concern because of the typically large amounts of anhedral. It may also be difficult to incorporate effective control surfaces without degrading the performance. The stability and control of conventional hypersonic vehicles are discussed in Refs. 16 and 17. Hui has published extensively on hypersonic stability and control (see Ref. 18), including the characteristics of caret wings.[15]

Few theoretical or numerical studies have included the effects of viscosity on waveriders. Bowcutt et al.[19] have included skin friction in their waverider optimization procedure. On slender vehicles such as these, it is very important to include viscous effects. Vehicles similar to Bowcutt's will be analyzed experimentally by NASA Langley Research Center in the near future[20] in order to evaluate viscous effects further. It would also be of interest to include displacement thickness effects in any analysis procedure; these are not included in Ref. 19. Since the boundary-layer thickness on a flat plate varies according to

$$(\delta/L)\alpha[(\gamma-1)M_\infty^2]/(2\sqrt{Re_\infty})$$

it can be orders of magnitude larger than at low Mach numbers. At high altitudes it can be of the same order as the thickness of a slender body.

The configurations in Ref. 19 were optimized for L/D and consequently have very small lift coefficients ($CL < 0.1$). The L/D is just one possible parameter that could be optimized. In addition, the contraints could also be varied. For some vehicles L/D will not be the most important parameter, such as those that go from Earth to orbit very rapidly without actually cruising. For these vehicles, one might be more interested in maximizing thrust minus drag ($T-D$) and thus aeropropulsion integration would be the main issue.

Classical waveriders are designed using known flowfields. The most common are the planar and conical flowfields of wedges and cones, respectively. These are not optimal shapes, even from an aerodynamic standpoint. Optimal hypersonic shapes are described in Refs. 21–23. Power law bodies have been shown to have very low drag compared to cones. With advanced computational methods, it should be possible to incorporate these low drag shapes into waveriders. Power law waveriders would have a Gothic-like planform and, consequently, would have significantly different leading-edge vortex flows at subsonic and supersonic speeds than a conical waverider with a delta planform. This could significantly alter the aerothermal heating and the low-speed vortex flows off the leading edge. Nonweiler[4] showed that rounding the apex of a delta planform would also help reduce the aerothermal heating at the apex. However, the power law bodies will have blunter nose cones, which may increase the total pressure losses to the inlets. Also, optimizing aerodynamic forces will be of little use if the vehicle's performance is governed mainly by aeropropulsion integration. Air-breathing hypersonic vehicles will be characterized as having lift, drag, moments, thrust, and trim all highly coupled.

In addition to being suboptimal aerodynamically, conical and planar flowfields are not optimum from a systems standpoint either. They present problems in terms of propulsion integration, control-surface location, and landing-gear placement. Their tremendous value comes in the guidance they give the designers. However, there has been little to guide the designers as to the effect of deviating from the conical or planar fields. Most studies have shown, however, that minor deviations from the classical shapes do not significantly alter the characteristics. This will be discussed in more detail in the Results section.

Since waveriders may be used as aerospace planes that take off and land horizontally on runways, their low-speed characteristics are also important. As with conventional highly swept wings, they can be expected to produce significant vortex lift at high angles of attack (subsonically and supersonically). However, the nature of these flowfields may differ significantly from delta wings because of the differences in thickness and planform.

As mentioned, the waverider off-design flowfield is not amenable to simple analyzes. Methods based on modified Newtonian or other component techniques (such as the Hypersonic Arbitrary Body Program[24]) are by definition incapable of modeling interference effects. Ideally, one would like to use the full Navier-Stokes equations, but this is expensive and not well validated at hypersonic speeds (particularly turbulence models and boundary-layer transition). For many problems, especially as a preliminary analysis, inviscid techniques can be quite useful. They cannot predict the important heat transfer and boundary-layer characteristics, but quantities such as surface pressure are often predicted very well with inviscid methods. This is especially true for vehicles that are relatively thick. Figure 1 shows that for relatively thick bodies, the skin friction has a negligible effect on the L/D.

However, Fig. 1 may not be applicable to higher Mach numbers because it does not show the effect of displacement thickness. The relative importance of the boundary layer on the outer flow can be estimated using the viscous interaction parameter: $\chi\alpha M_\infty^3/\sqrt{Re_\infty}$. When this parameter is order unity or larger, the surface pressure distribution may differ significantly from inviscid predictions. At Mach = 10, the interactions may be significant when the Reynolds number is $< 1 \times 10^6$. If a vehicle is designed for high-altitude flight (where the aerothermal heating will be reduced), the Reynolds number most likely will be smaller than these numbers. When these effects are large, the inviscid methods must be abandoned or at least coupled to a boundary-layer routine. However, at hypersonic speeds, the concept of an inner viscous flow and an outer inviscid flow is not always valid.

At high Mach numbers and/or low Reynolds numbers, rarefied gas effects will also become important. These flows are usually characterized by the Knudsen number ($Kn = \lambda/L$), where λ is the mean free path and L is some characteristic length [e.g., $L = \rho(dx/d\rho)$]. The Euler equations are valid in the limit as $Kn \to 0$, and the Navier-Stokes for $Kn \ll 1$. Typically, when $Kn > 0.1$, one must resort to kinetic-theory-based methods such as the direct simulation Monte Carlo method.[25] As the Knudsen number is increased, shock waves become thicker and thicker. Therefore, at high altitudes, the concept of capturing a bow shock on a leading edge becomes somewhat arbitrary. This means that waverider performance will be reduced due to the inability to capture the high-pressure air. The performance of waveriders under these circumstances has not been investigated in detail. An important point to make is that, although in the freestream $Kn \simeq M/Re$, near stagnation regions $Kn \simeq 1/(MRe)$; therefore surface quantities can often be predicted quite well with continuum theories.

Method

In the present study, a numerical method based on the nonlinear Euler equations has been used. These equations accurately model the effects of strong shock waves (not internal shock wave structure, however) and vorticity transport. In addition, when the separation point is fixed, such as at a sharp leading edge, they have been shown to predict separated flows reasonably well. Relatively thick bodies will be analyzed here

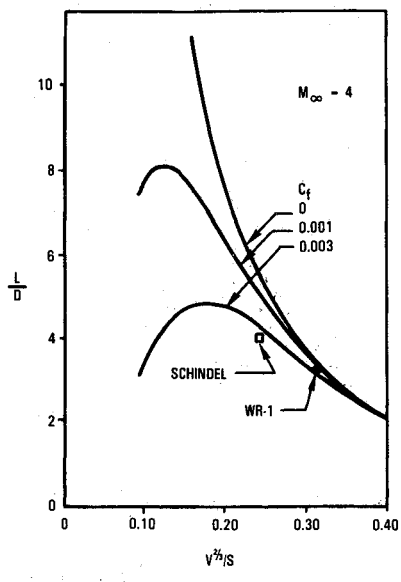

Fig. 1 Effect of skin friction and thickness on L/D.[33]

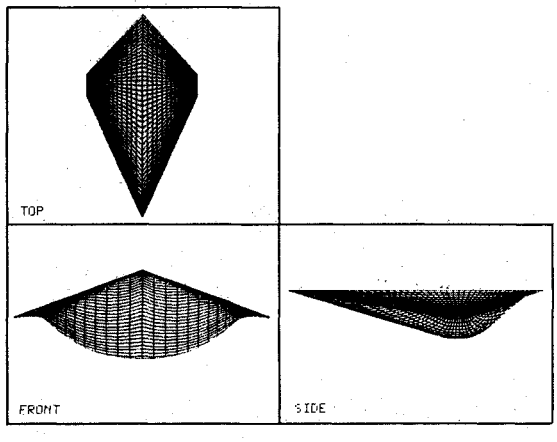

Fig. 2 Three views of Rasmussen's elliptical cone waverider with base (WR-1).

(forebody thickness/chord = 0.21 and 0.30), so inviscid methods should be fairly accurate. These types of bodies will be of interest when large amounts of volume are required for payload or fuel. For example, hydrogen-powered vehicles may require relatively thick fuselages due to the low density of liquid hydrogen compared to conventional fuels.[3]

The results presented here were all obtained using the Lockheed Three-Dimensional Euler Navier-Stokes Aerodynamic Method (TEAM), the development of which was partially funded by the United States Air Force. This computer program is based on the FLO-57 algorithm developed by Jameson et al.[26] Lockheed has made major refinements to the method over the past several years.[27-29]

In the TEAM code, the region surrounding a given configuration is subdivided into small cells. In each of the cells, the time-dependent Euler (or Navier-Stokes) equations (in integral equation form), representing mass, momentum, and energy conservation,

$$\frac{\partial}{\partial t}\int\int\int Q \, dV = -\int\int (F\,\bar{V}\cdot\hat{n} + G)\, dS$$

where

$$Q = \begin{bmatrix} \rho \\ \rho\ \bar{V} \\ \rho\ E \end{bmatrix}, \quad F = \begin{bmatrix} \rho \\ \rho\ \bar{V} \\ \rho\ H \end{bmatrix}, \quad G = \begin{bmatrix} 0 \\ p\ \hat{n} \\ 0 \end{bmatrix}$$

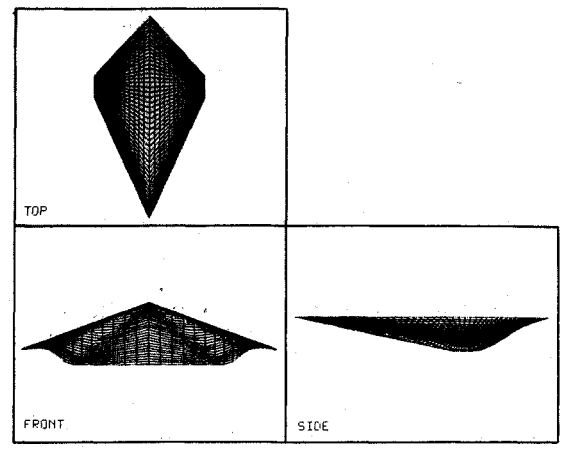

Fig. 3 Three views of flat-bottom waverider with base (WR-2).

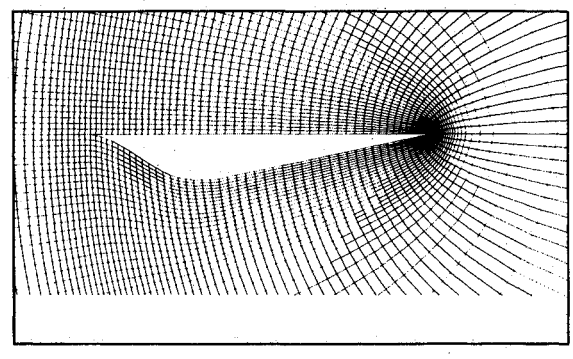

Fig. 4 Sample computational grid at plane of symmetry for WR-2.

are integrated in time using a multistage Runge-Kutta scheme. The quantities represented by ρ, V, p, e, and h are density, velocity, pressure, total energy, and total enthalpy, respectively. Notice that density, momentum, and energy are all calculated from the time-stepping process; pressure and enthalpy are required for the flux terms. For perfect gases, pressure is normally calculated using a form of the energy equation and then enthalpy is calculated from $H = p/\rho + E$. In simulating a real gas in equilibrium, one must calculate pressure, enthalpy, specific heat ratio, and the speed of sound (required for upwind schemes) properly; for example, by using the subroutines described in Ref. 30. For nonequilibrium chemistry, one must add additional equations to the time-stepping procedure that govern the species concentrations. Nonequilibrium effects are not included in the TEAM code at this time.

To accelerate convergence to the steady state, local rather than global time steps are used. This will produce valid steady-state results when there is a steady-state solution. For unsteady flows, one must use the code in a time-accurate mode, which is quite expensive. Implicit residual smoothing[31] further reduces the number of time steps required to reach the steady state. Appropriate nonreflecting boundary conditions based on Riemann invariants[31] are used at the far-field boundaries and no normal-flow conditions are used on the solid surface. Upwind differencing based on a Riemann solver[32,33] has also been incorporated and can be used instead of the standard adaptive artificial dissipation. The upwind differencing increases the robustness of the program, but does require more computer time.

The finite-volume formulation essentially decouples the flow solver from the grid generator. The grids can be constructed in any convenient manner; only the Cartesian coordinates of the nodal points are required by the solver. The present version of the solver can accommodate multiple, patched zonal grids of arbitrary topologies. This is a necessity for

analyzing realistic complete aircraft configurations. The original FLO-57 solver was limited to isolated wings having C-H grids, whereas the O-O and C-O types offer improved resolution. The letters C, H, and O refer to the way the grid looks in the spanwise and chordwise directions. A C-H grid wraps around the airfoil section like a C, and has these two-dimensional grids stacked up in the spanwise direction to form the region around the wing. Thus, from the front, a C-H grid looks like an array of Hs. If a C-H mesh is used, adequate resolution near the wing tip can be obtained only by increasing the number of cells in the spanwise direction. It must be noted that none of these topologies is as suitable as the H-H when the detailed flowfield is desired about all sections of a wing-body or wing-body-tail configuration.

The finite volume grids used here were all of the C-H type. Several different grids were used; a typical grid had $105 \times 29 \times 25$ cells (76,125) in the chordwise, normal, and spanwise directions, respectively. For the subsonic cases, the far-field boundary was several vehicle lengths away from the body surface; for supersonic flows, the far-field boundary was much closer (although still in the freestream). Other than this, no attempt was made to tailor the grid to the particular flowfield. Similar grids were used at most Mach numbers, which means they could not have been optimal for all Mach numbers. Ideally, one would like to cluster cells near shocks, but shockwave location and strength changes with Mach number. Therefore, a new grid would be required at each Mach number, which would have been extremely time consuming. Some type of adaptive grid scheme would have been useful, but is currently not available in the TEAM code. However, the grids used were relatively dense and should yield reasonable results for forces and moments at most Mach numbers.

Depending on which options are used, the TEAM code requires about 0.00002 CPU s/cycle/cell on a Cray XMP-24. For the results presented here, 400–3000 cycles were required to reduce the residual error by three to four orders of magnitude. The convergence rate varied dramatically with Mach number. At the very high Mach numbers, where the shocks are very close to the body and not resolved well, the code converged extremely rapidly. Likewise, for coarse meshes, the code converged very rapidly. In principle, this should allow preliminary investigations to be made of configurations very quickly, with detailed examinations performed afterwards. In

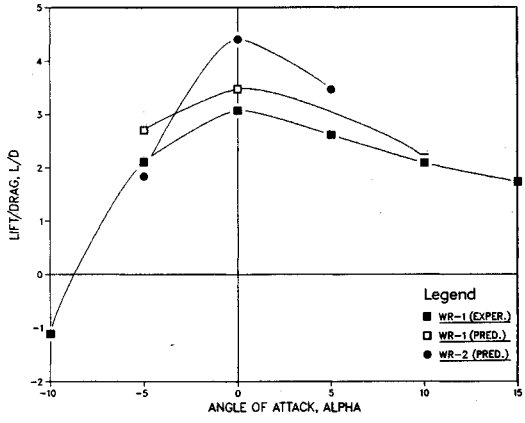

Fig. 5 Experimental and predicted L/D for various angles of attack, Mach = 4.

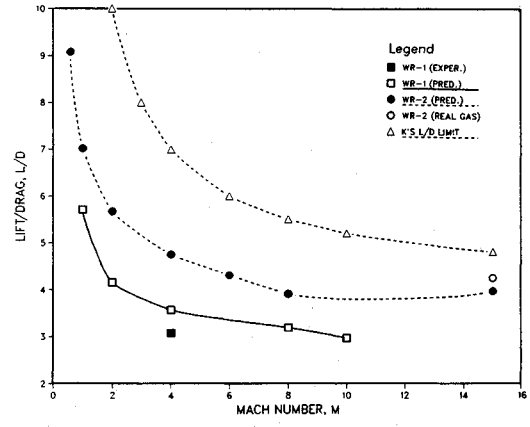

Fig. 6 Experimental and predicted L/D for various mach numbers, $\alpha = 0$.

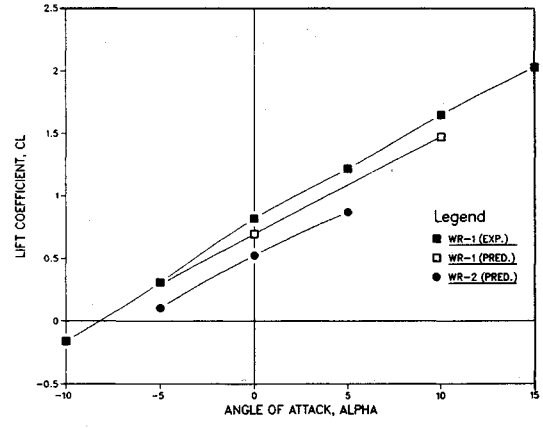

Fig. 7 Experimental and predicted lift coefficients for various angles of attack, Mach = 4.

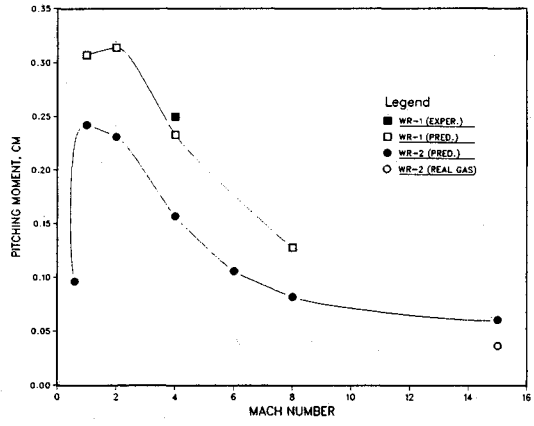

Fig. 8 Experimental and predicted pitching moment coefficients for various Mach numbers, $\alpha = 0$.

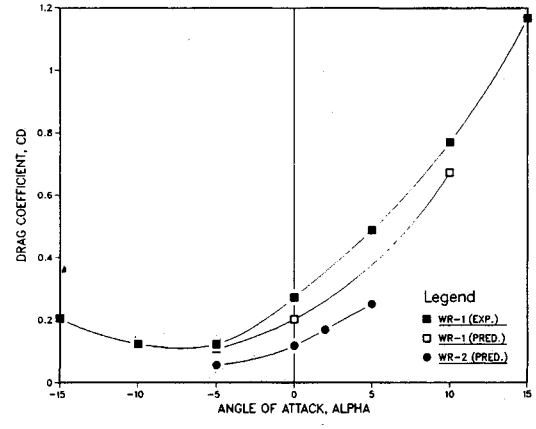

Fig. 9 Experimental and predicted axial force coefficients for various angles of attack, Mach = 4.

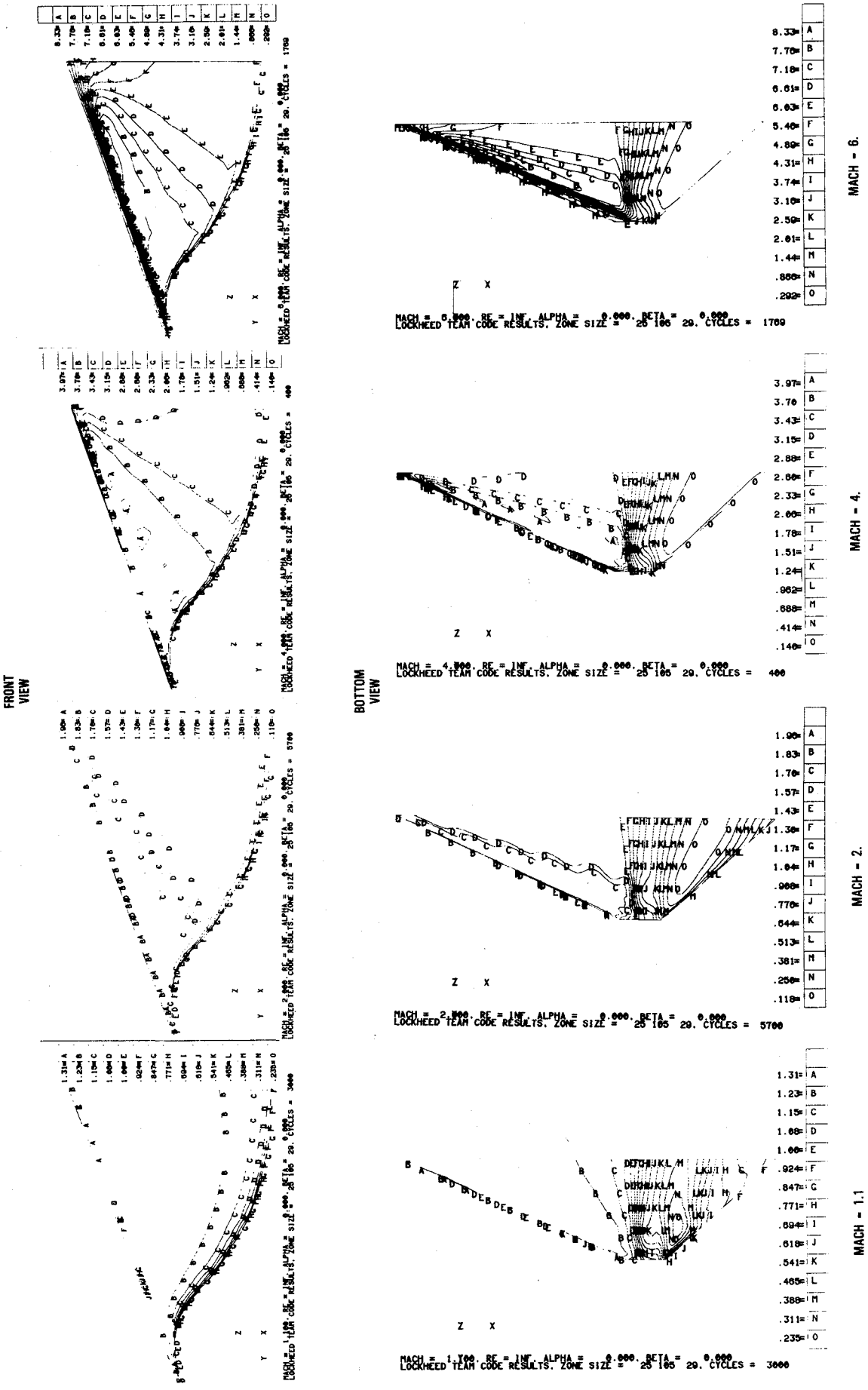

Fig. 10 Pressure distributions (p/p_∞) over WR-1 at Mach = 1.1, 2, 4, and 6, angle of attack = 0.

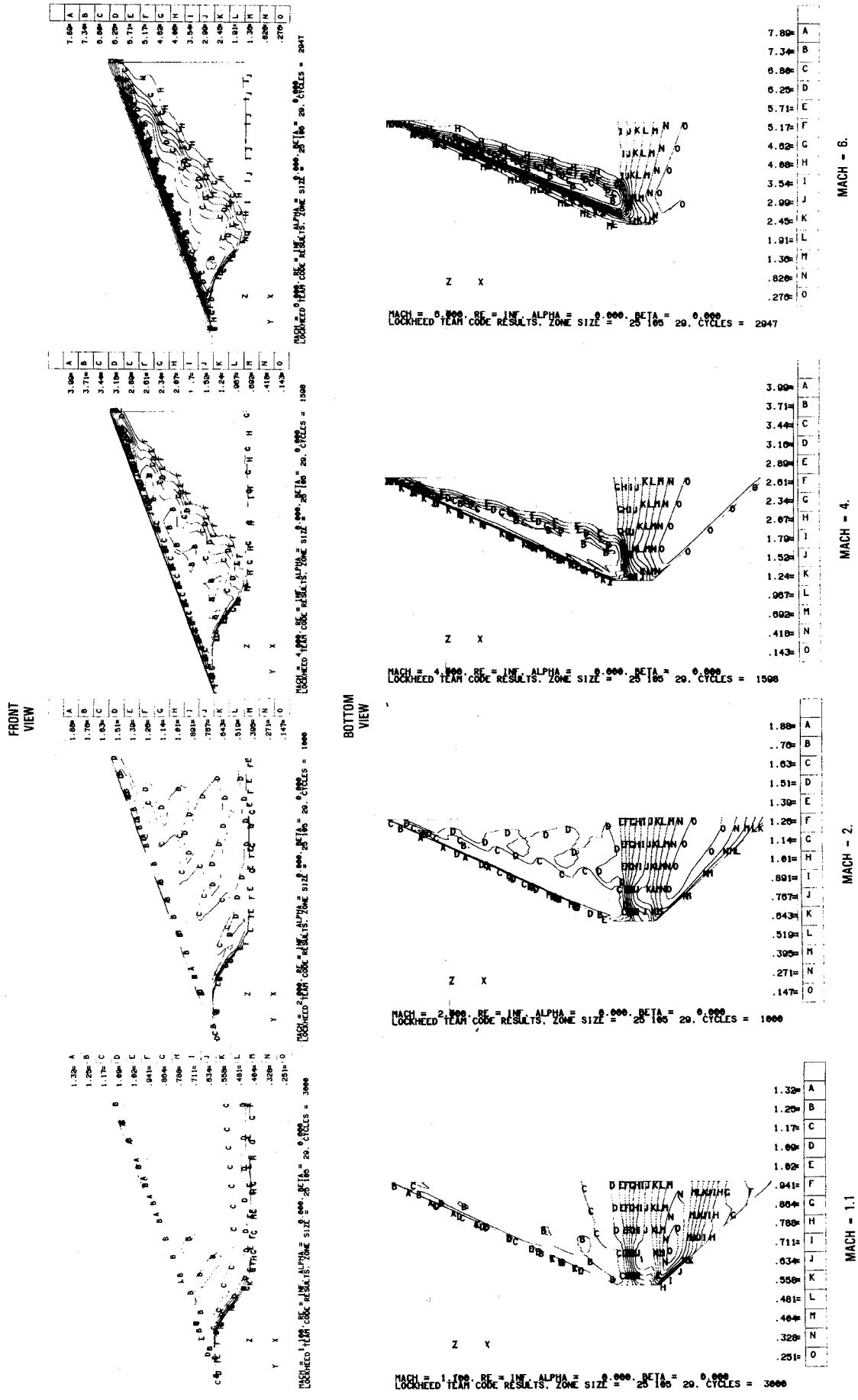

Fig. 11 Pressure distributions (p/p_∞) over WR-2 at Mach = 1.1, 2, 4, and 6, angle of attack = 0.

some cases, the solutions were restarted from previous runs, which did allow some savings in computer time.

Results

Two configurations were investigated here. The first one (referred to here as WR-1) is the Rasmussen et al. elliptical-cone waverider[34] shown in Fig. 2. This configuration has 20 deg of anhedral and a leading-edge sweep of 65.53 deg. The second configuration (WR-2) is a flat-bottomed version of Rasmussen's waverider (Fig. 3). WR-2 was obtained by simply cutting off the underside of WR-1. The section removed was cut away by a plane perpendicular to the plane of symmetry and at an angle of -11.95 deg to the freestream direction. Whereas the wind-tunnel model of WR-1 had a 18.06 cm base height, the base height of WR-2 would be 12.7 cm. The length of both of them is 60.0 cm (excluding the fairing at the base). Note that WR-2 should be called a pseudowaverider since the shock will not be exactly attached to the leading edge.

The shape of WR-2 was chosen because it represents a deviation from the standard conical flowfield. The flat underside is desirable from a practical standpoint. Both landing gear and inlets may be easier to incorporate into a flat surface. It was also reasoned that the shock wave attached to the leading edge may not be affected too much by relieving the pressure on the very bottom and, thus, the flow may still be fairly well contained. If this were true then the bottom portion of WR-1 might contribute more to the drag than to the lift. In addition, WR-2 should have both lower friction drag and base drag because it has a smaller wetted area and base area than WR-1.

In order to evaluate realistic vehicles, a fairing was added to the aft end of WR-1 and WR-2. This is shown in Fig. 4, which is a typical grid at the plane of symmetry. This fairing is aligned with the freestream on the upper surface. The lower surface consists of a flat (aligned with upper surface) portion whose length is 10% of the local chord and then a cosine shaped portion that is an additional 50% of the local chord. Thus the total length of the fairing is 60% of the local chord. However, in order to compare to Rasmussen's data directly, the force and moment calculations presented later do not include the forces and moments on the fairing. Since, on an actual configuration, the aft-end flow would be dominated by jet exhaust entrainment and/or separated wake flow, the inviscid contributions were not added to the forebody forces and moments. In the near future, viscous analyses will be performed on these configurations by solving the Reynolds-averaged Navier-Stokes equations, and the flow in the base region will be of great interest.

WR-1 was designed for Mach 4 and 0-deg angle-of-attack, where its L/D is a maximum. Experimental and predicted values of L/D (at Mach 4) are shown in Fig. 5. The experimental results for WR-1 compare fairly well considering no viscous effects are included, but this should not be a surprise since it is a relatively thick body. The L/D for WR-2 is substantially higher than WR-1, mainly because the parameter $V^{**}(2/3)/S$ is smaller (see Fig. 3). Therefore, the flattening of the standard Rasmussen waverider would be beneficial from a systems (inlets, landing gear, etc.) viewpoint, and the L/D is higher. The L/D vs Mach number is shown in Fig. 6. The flattened waverider has a higher L/D over the entire Mach number range. Also plotted is Kuchemann's L/D limit of $4(M_\infty + 3)/M_\infty$. The performance of both WR-1 and WR-2 is significantly below this limit.

The lift coefficient (CL) vs angle of attack is shown in Fig. 7 for Mach = 4. These results show good agreement between experiment and theory for WR-1. The behavior is virtually linear for both WR-1 and WR-2. Pitching moment (CM) vs Mach number (including the one experimental data point available) is shown in Fig. 8. Figure 9 shows the inviscid drag or axial force (minus base drag). The experimental and predicted values compare well and WR-2 has less drag than WR-1. Note that the reference lengths and areas used here are the same as used in Ref. 31, i.e., $L = 60$ cm and $A = 489.22$ cm^2.

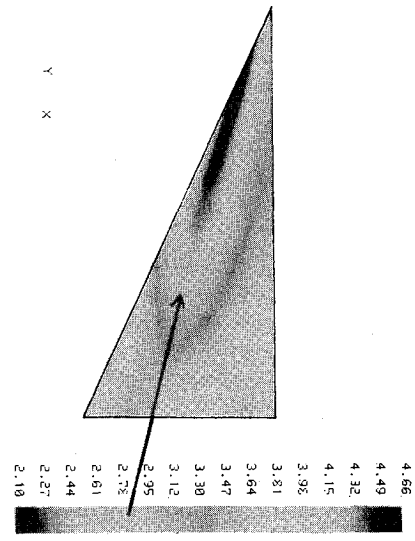

Fig. 12 Pressure distribution for subsonic flow over WR-2 at Mach = 0.6 and angle of attack = 20 deg.

Table 1 Forebody forces and moments, $M_\infty = 15$

Gas	Lift coefficient	Drag coefficient	Pitching moment	Lift/drag
Perfect	0.305	0.077	0.061	3.96
Real	0.288	0.072	0.059	4.00[a]
% Difference	−5.6	−6.5	−3.3	1.00

[a]at 40 km

The reference area used here is the base area of WR-1 (as in Ref. 31) and is not the planform area (which is 1638.16 cm^2).

For highly three-dimensional flowfields such as these, it is instructive to use three-dimensional color graphics (reproduced here as contour plots) to interpret the results. Figures 10 and 11 show pressure distributions on front and bottom views of WR-1 and WR-2, respectively, at Mach numbers of 1.1, 2, 4, and 6.0, respectively ($\alpha = 0$). All pressures shown here are nondimensionalized by the freestream pressure (p/p_∞). For both waveriders, at Mach = 2, 4, and 6, the flowfield appears to be quite conical. In addition, the flat bottom waverider (WR-2) shows a very uniform pressure distribution on the underside, which would be desirable for modular inlet installation.

The wavy patterns near the edge of the flat underside are due to minor waves in the surface definition. The numerical method is very sensitive to geometry variations, and the grid generation scheme used here (parabolic conformal mapping) is not as effective on these highly swept planforms as one would like. This could be corrected by specifying the body with more points or by using a different type of grid generation scheme. An H-O grid would allow better shock capturing because the grid could more easily be aligned with the shocks. However, the present type of grid is well suited to transonic and subsonic flows.

At higher Mach numbers, one simply cannot use a perfect gas model because it predicts pressures and temperatures that are unrealistically high. The previously described code was used to predict the flowfield around WR-2 at Mach = 15 and $\alpha = 0$ using a perfect gas model and a real gas model (40 km), respectively. The surface pressures are lower than that predicted by the perfect gas relations, and this causes the forces and moments to differ also (see Table 1). These effects are small because of the slender nature of the body, especially the small leading-edge radii.

For many applications, these waveriders will be required to fly through all four speed regimes (subsonic, transonic, supersonic, and hypersonic); therefore, it is important to know the behavior of these configurations over the entire range. The

only subsonic flowfield that will be shown here is Fig. 12. As mentioned, one can expect significant vortex flows from these configurations at high angles of attack. Figure 12 shows the pressure distribution on the upper surface of WR-1 at Mach = 0.6 and $\alpha = 20$ deg. The low-pressure region can be attributed to a leading-edge vortex. Vortices such as these occur at supersonic speeds also and can lead to significant aerothermal heating problems.

Conclusions

The preceding results for the waverider are very encouraging because most design methods for hypersonic vehicles are incapable of predicting waverider performance. This is especially true for off-design performance where only a truly nonlinear prediction method is adequate. Because waveriders are based on favorable interference, methods such as the Hypersonic Arbitrary Body Program[24] cannot be used. For lower Reynolds number, higher Mach numbers, or more slender vehicles, the viscous effects will become more important and the inviscid CFD methods must be replaced by Navier-Stokes and Boltzmann methods.

Acknowledgments

This work was funded by Air Force Contract F33615-84-C-3005 and Lockheed Aeronautical Systems Company.

References

[1]Rasmussen, M. L., and Clement, L. W., "Cone-Derived Waveriders with Longitudinal Curvature," *Journal of Spacecraft and Rockets,* Vol. 23, No. 5, 1986, pp. 461–469.

[2]Kuchemann, D., *The Aerodynamic Design of Aircraft,* Pergammon, New York, 1978.

[3]Gregory, T. J., Peterson, R. H., and Wyss, J. A., "Performance Tradeoffs and Research Problems for Hypersonic Transports," *Journal of Aircraft,* Vol. 2, No. 4, 1965, pp. 266–271.

[4]Nonweiler, T. R. F., "Aerodynamic Problems of Manned Space Flight," *Journal of the Royal Aerospace Society,* Vol. 63, 1959, pp. 521–528.

[5]Schindel, L. H., "Tactical Missile Aerodynamics," *AIAA Progress in Astronautics and Aeronautics: Tactical Missile Aerodynamics*, Vol. 104, edited by M. S. Hemsch and J. N. Nielsen, AIAA, New York, 1986.

[6]Townend, L. H., "Some Design Aspects of Space Shuttle Orbiters," *Progress in Aerospace Sciences,* Vol. 13, Pergammon, Oxford. (See also: "The Waverider," *Hypersonic Aerothermodynamics,* Von Kármán Institute, Lecture Series 1984-01, Feb. 1984.)

[7]Bogdonoff, S. M. (ed.), "Hypersonic Boundary Layers and Flow Fields," AGARD Specialists Meeting of the Fluid Dynamics Panel, CP-30, May 1968.

[8]Squire, L. C., "A Comparison of the Lift of Flat Delta Wings and Waveriders at High Angles of Incidence and High Mach Numbers," *Ingenieur-Archiv,* Vol. 40, No. 5, 1971, pp. 339–352.

[9]Jones, K. M., "Application of a Supersonic Full Potential Method for Analysis of Waverider Configurations," NASA TP-2608, Sept. 1986.

[10]Hunt, J. L., Johnston, P. J., and Riebe, G. D., "Flow Fields and Aerodynamic Characteristics for Hypersonic Missiles with Mid-Fuselage Inlets," AIAA Paper 83-0542, Jan. 1983.

[11]Hemdan, H. T., and Jischke, M. C., "Inlets for Waveriders Derived from Elliptic-Cone Stream Surfaces," *Journal of Spacecraft and Rockets,* Vol. 24, No. 1, 1987.

[12]Korkegi, R. H., "Survey of Viscous Interactions Associated with High Mach Number Flight," *AIAA Journal,* Vol. 9, No. 5, 1971.

[13]Holden, M. H., "A Review of Aerothermal Problems Associated with Hypersonic Flight," AIAA Paper 86-0267, Jan. 1986.

[14]Venn, J., and Flower, J. W., "Shock Patterns for Simple Caret Wings," *Aeronautical Journal of the Royal Aerospace Society,* Vol. 74, No. 712, April, 1970.

[15]Settles, G. S., and Dolling, D. S., "Swept Shock Wave/Boundary Layer Interactions," *Progress in Astronautics and Aeronautics: Tactical Missile Aerodynamics,* Vol. 104, edited by M. S. Hemsch and J. N. Nielsen, AIAA, New York, 1986.

[16]Drummond, A. M., "Performance and Stability of Hypervelocity Aircraft Flying on a Minor Circle," *Progress in Aerospace Sciences,* Vol. 13, edited by D. Kuchemann, Pergammon, Oxford, 1972.

[17]East, R. A., "Hypersonic Static and Dynamic Stability, Part II: Inviscid Prediction Methods for Unsteady Hypersonic Flow," *Hypersonic Aerothermodynamics,* Von Kármán Institute, Lecture Series 1984-01, Feb. 1984.

[18]Hui, W. H., "Stability of Oscillating Wedges and Caret Wings in Hypersonic and Supersonic Flows," *AIAA Journal,* Vol. 7, No. 8, 1969.

[19]Bowcutt, K. G., Anderson, J. D., and Capriotti, D., "Viscous Optimized Hypersonic Waveriders," AIAA Paper 87-0272, Jan. 1987.

[20]Bauer, S. X. S., "Application of Hypersonic Waverider Optimization Method," AIAA Paper 87-0644, Jan. 1987.

[21]Spencer, B., and Fox, C. H., "Experimental Studies of Optimum Body Shapes at Hypersonic Speeds," *Journal of Astronautical Sciences,* Vol. 14, No. 5, 1967.

[22]Cole, J. D., and Zien, T. F., "A Class of Three-Dimensional, Optimum Hypersonic Wings," *AIAA Journal,* Vol. 7, No. 2, 1969.

[23]Kim, B. S., Rasmussen, M. L., and Jischke, M. C., "Optimization of Waverider Configurations Generated from Axisymmetric Conical Flows," *Journal of Spacecraft and Rockets,* Vol. 20, No. 5, 1983.

[24]Gentry, A. E., "Hypersonic Arbitrary Body Aerodynamic Computer Program Mark II Version, Vol. I—User's Manual," Douglas Aircraft Corp., Long Beach, CA, Rept. DAC 61552, April 1968.

[25]Bird, G. A., *Molecular Gas Dynamics,* Clarendon, Oxford, 1976.

[26]Jameson, A., Schmidt, W., and Turkel, E., "Numerical Solutions of the Euler Equations by Finite Volume Methods Using Runge-Kutta Time-Stepping Schemes," AIAA Paper 81-1259, June 1981.

[27]Raj, P., and Long, L. N., "An Euler Aerodynamic Method for Leading-Edge Vortex Flow Simulation," NASA CP-2416, Oct. 1985.

[28]Raj, P., and Brennan, J., "Improvements to an Euler Aerodynamic Method for Transonic Flow Analysis," AIAA Paper 87-0040, Jan. 1987.

[29]Raj, P., Olling, C. R., Sikora, J. S., Keen, J. M., Singer, S. W., Brennan, J. E., and Long, L. N., "Three-Dimensional Euler/Navier-Stokes Aerodynamic Method (TEAM)," Vols. I, II, and III, AFWAL-TR-87-3074, June 1989.

[30]Srinivasan, S., Tannehill, J. C., and Weilmuenster, K. J., "Simplified Curve Fits for the Thermodynamic Properties of Equilibrium Air," Iowa State Univ., Ames, Iowa, ISU-ERI-Ames-86401, June 1986.

[31]Jameson, A., and Baker, T. J., "Solution of the Euler Equations for Complex Configurations," AIAA Paper 83-1929, July 1983.

[32]Roe, P. L., "Approximate Riemann Solvers, Parameter Vector, and Difference Schemes," *Journal of Computational Physics,* Vol. 43, 1981, pp. 357–372.

[33]Gnoffo, P. A., "Application of Program LAURA to Three-Dimensional AOTV Flowfields," AIAA Paper 86-0565, Jan. 1986.

[34]Rasmussen, M. L., Jischke, M. C., and Daniel, D. C., "Experimental Forces and Moments on Cone-Derived Waveriders for $M = 3$ to 5," *Journal of Spacecraft and Rockets,* Vol. 19, No. 6, 1982, pp. 592–598.